

Numerical simulations of microquasar jets

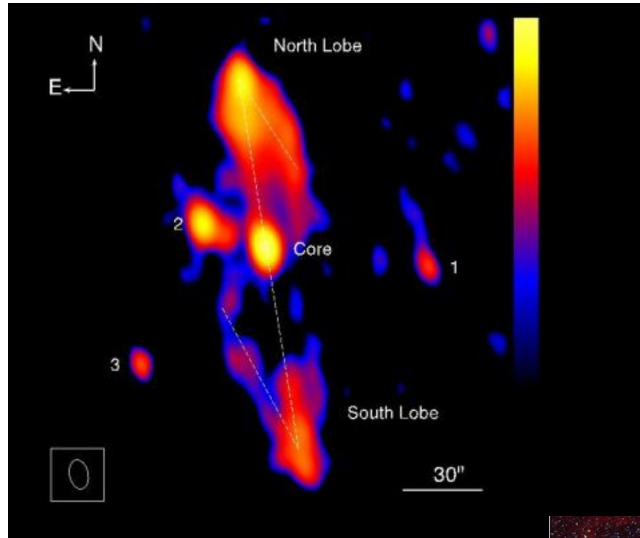
Manel Perucho Pla

Departament d'Astronomia i Astrofísica / Observatori Astronòmic
Universitat de València

colls. Valentí Bosch-Ramon, Jose López-Miralles, Pol Bordas, Dmitry Khangulyan, Josep Maria Paredes, José María Martí, Simone Migliari

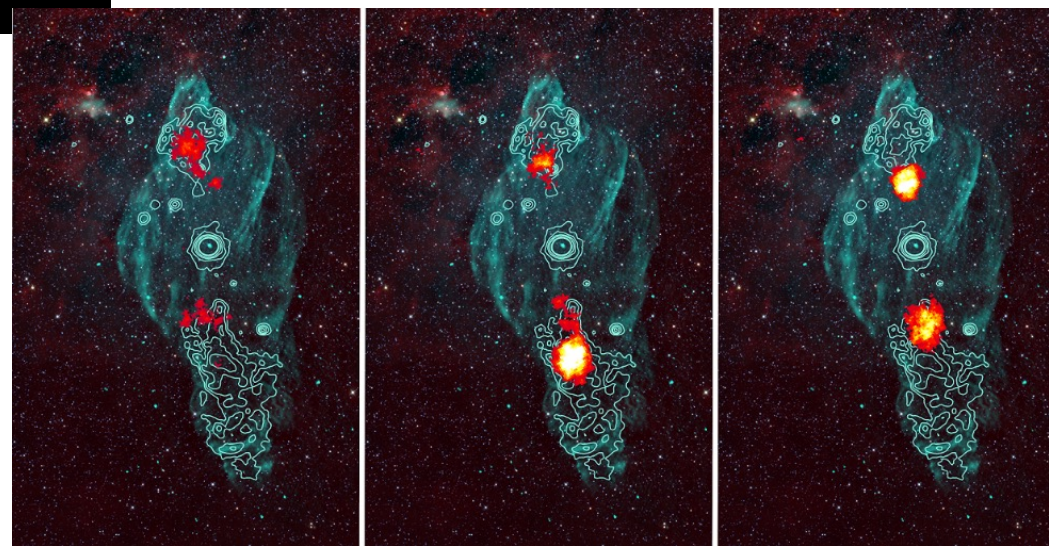
Variable Galactic Gamma-Ray Sources, Barcelona, May 2025

jets in microquasars

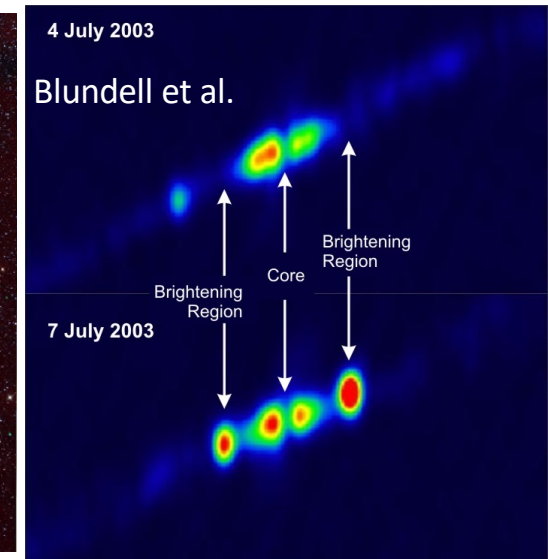
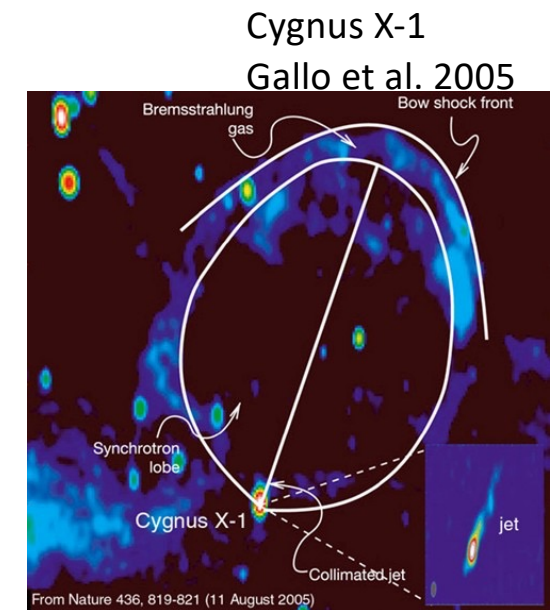


~20 sources with detected jets
(microquasars) in the galaxy
(Massi '05, Ribó '05).

SS 433. Golap, M.G.; Wide Field Survey Explorer (WISE); X-rays (ROSAT/M. Brinkmann; TeV: H.E.S.S.)



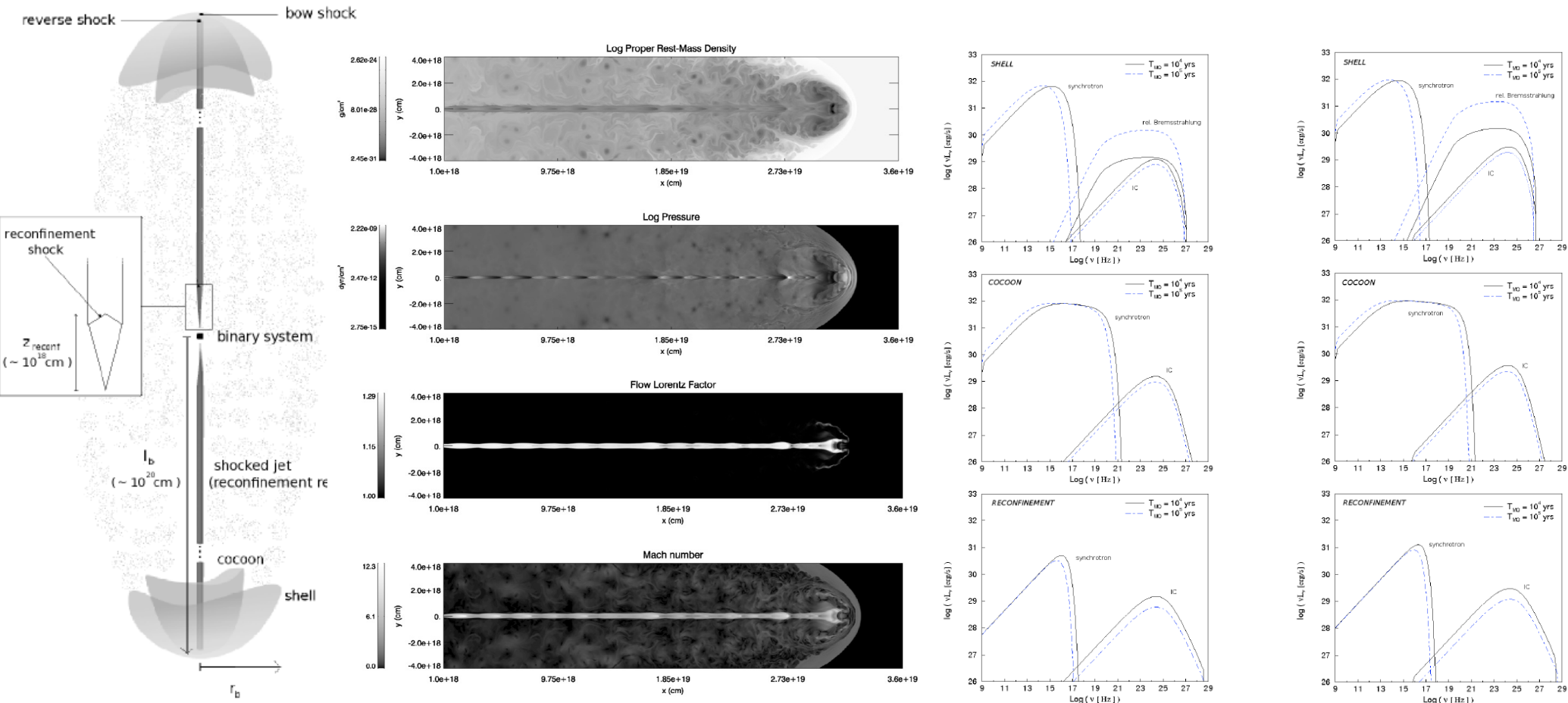
GRS 1758-258
Martí et al. 2018



4 July 2003
Blundell et al.
7 July 2003

Simulations of jets in high-mass microquasars

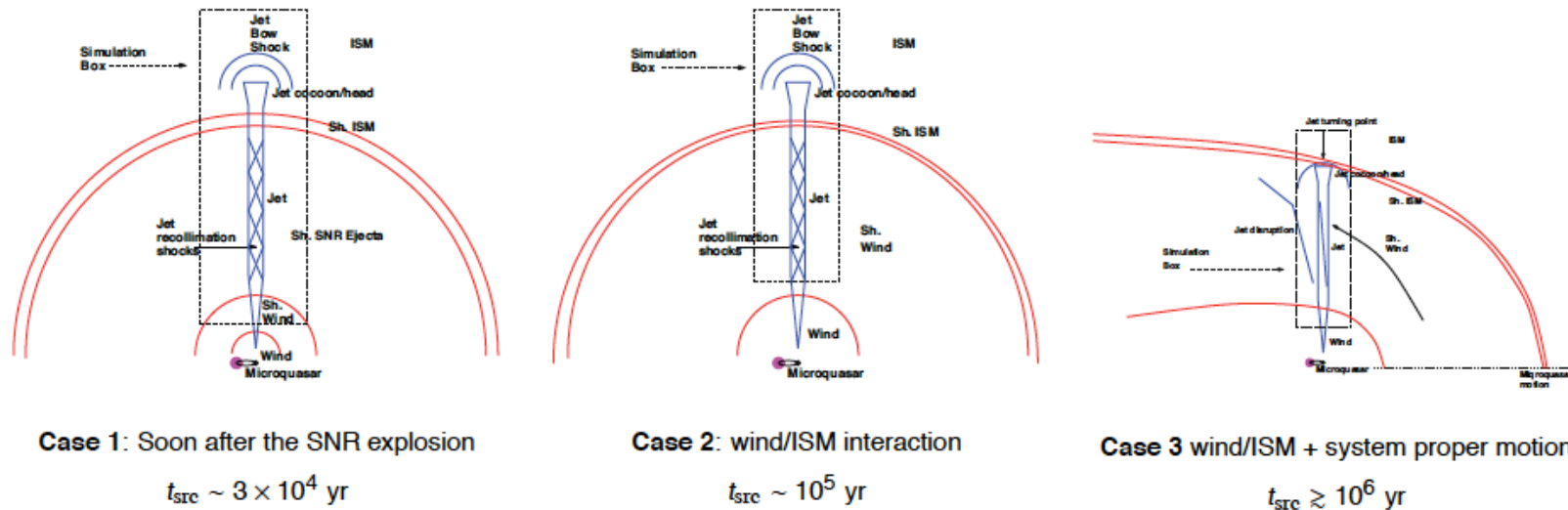
Long-term evolution of microquasar jets



Bordas, Bosch-Ramon, Paredes, MP 2009.

Simulations of jets in high-mass microquasars

Long-term evolution of microquasar jets



Numerical simulations

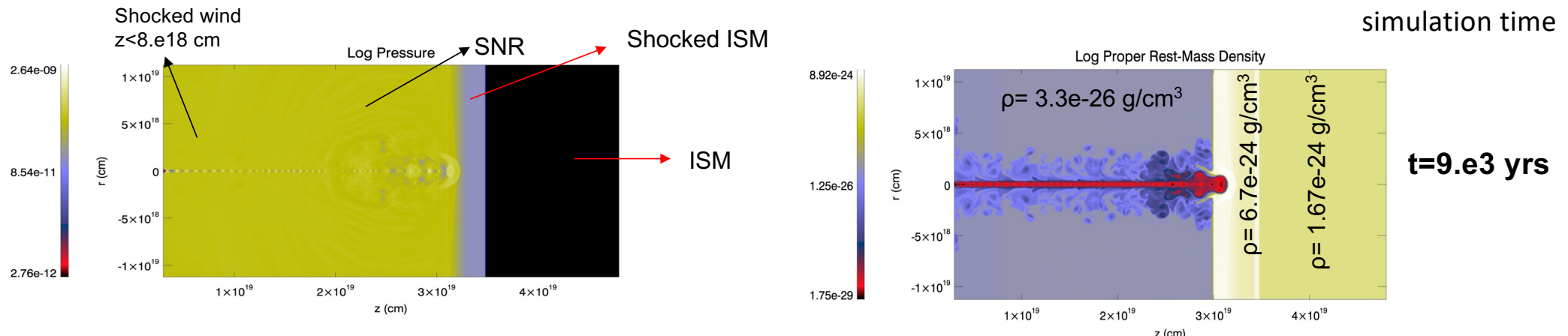
	Case 1	Case 2	Case 3
Jet power	$3 \times 10^{36} \text{ erg s}^{-1}$	$3 \times 10^{36} \text{ erg s}^{-1}$	$3 \times 10^{36} \text{ erg s}^{-1}$
Injection point z_0	$3 \times 10^{18} \text{ cm}$	$3 \times 10^{18} \text{ cm}$	$1.25 \times 10^{18} \text{ cm}$
Initial jet radius	$0.1 z_0$	$0.1 z_0$	$1.5 \times 10^{17} \text{ cm}$
Jet velocity	$10^{10} \text{ cm s}^{-1}$	$10^{10} \text{ cm s}^{-1}$	$10^{10} \text{ cm s}^{-1}$
Jet Mach number	18	18	18
Jet mass density	$1.8 \times 10^{-29} \text{ gr cm}^{-3}$	$1.8 \times 10^{-29} \text{ gr cm}^{-3}$	$8.3 \times 10^{-29} \text{ gr cm}^{-3}$

Bosch-Ramon, MP & Bordas, 2011

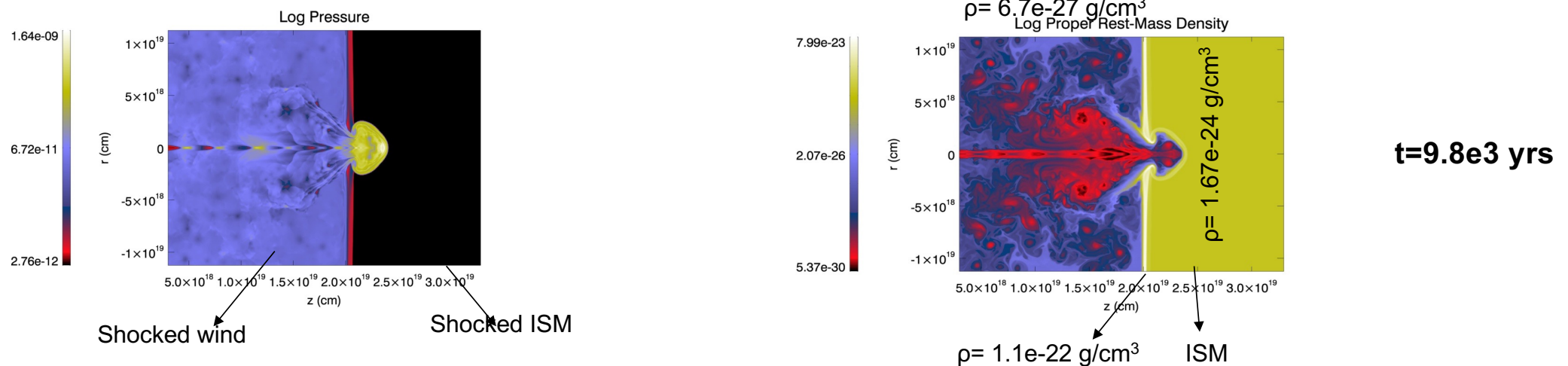
Simulations of jets in high-mass microquasars

Long-term evolution of microquasar jets

Case 1: young MQ ($t < 1.e5$ yrs), inside the hot SNR.



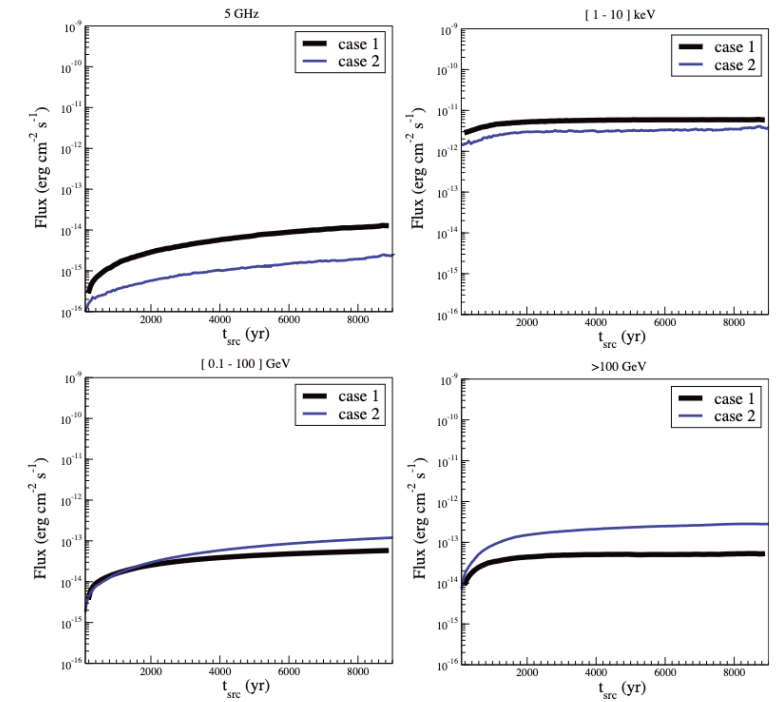
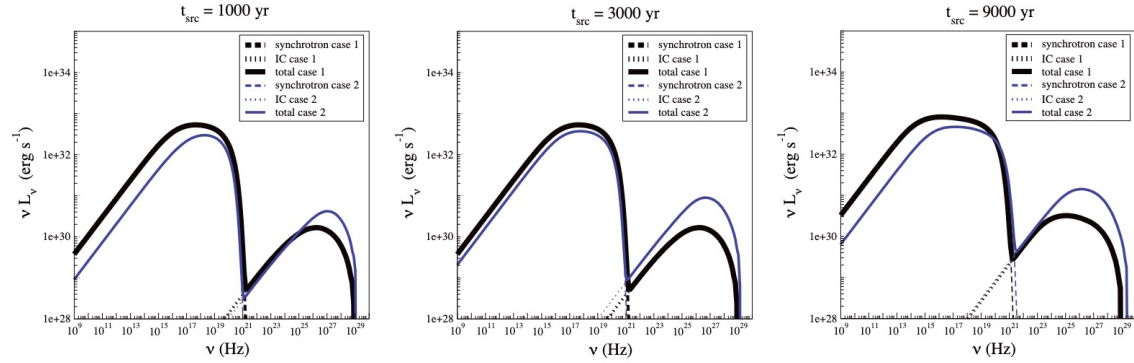
Case 2: older MQ ($t \sim 1.e5$ yrs), the SNR has dissipated and the jet propagates in the wind-wind/ISM shock-ISM



Simulations of jets in high-mass microquasars

Long-term evolution of microquasar jets

At 3 kpc:



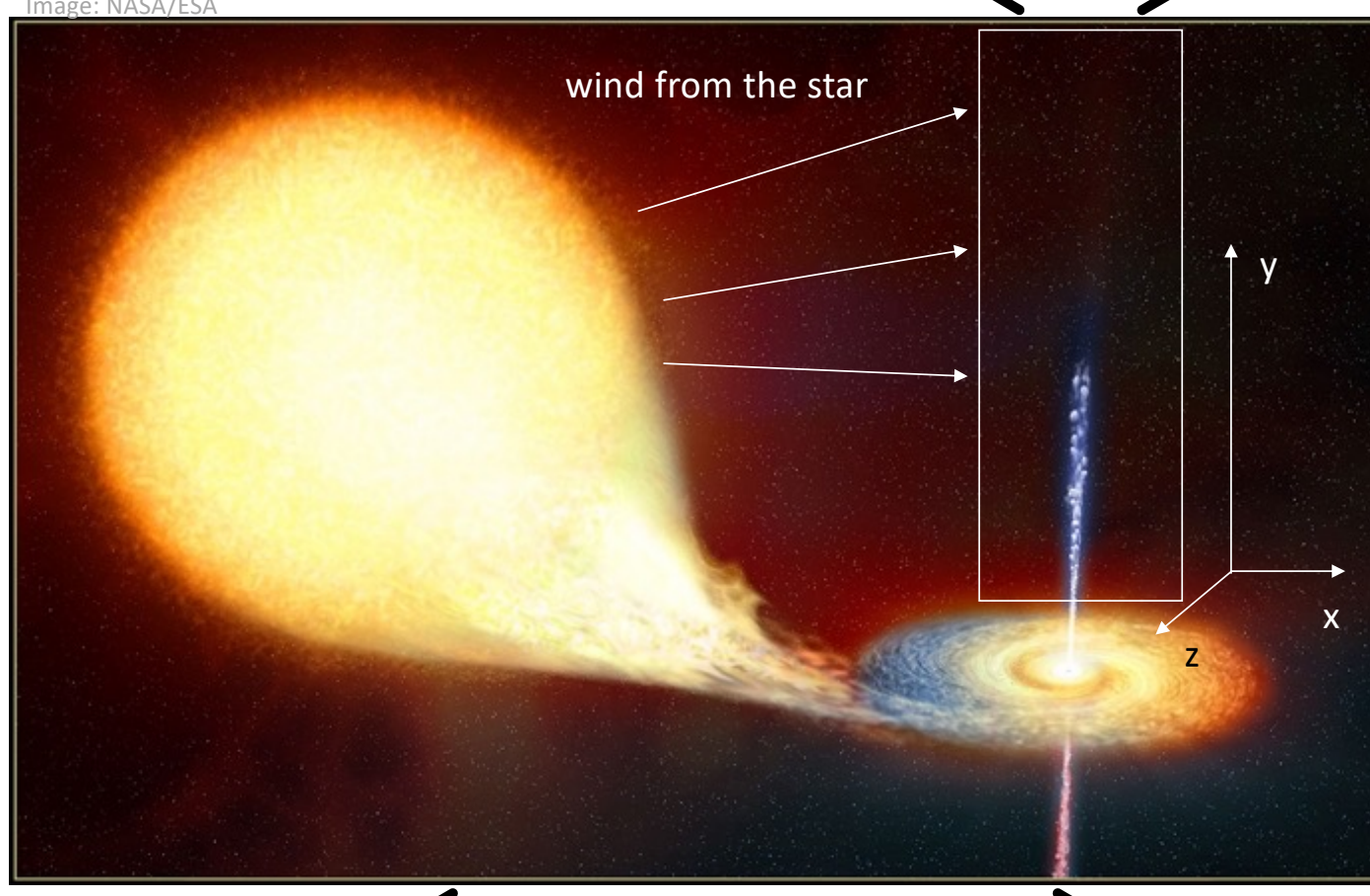
Hard X-rays and gamma rays could reveal the presence of microquasar jets interacting with the ISM.

Fig. 15. Evolution of the computed fluxes at 5 GHz (*top, left*), 1–10 keV (*top, right*), 0.1–100 GeV (*bottom, left*), and >100 GeV (*bottom right*) up to 10^4 yr, for cases 1 (black/thick lines) and 2 (blue/thin lines).

RMHD simulations of microquasar jets: stability

Wind-jet interaction in massive X-ray binaries

Image: NASA/ESA



$2 \ 10^{12} \text{ cm}$
 $\sim 0.13 \text{ AU}$

$6 \ 10^{10} \text{ cm}$
 $\sim 0.004 \text{ AU}$

$R_{\text{orb}} \sim 2 \ 10^{12} \text{ cm}$

injection times much shorter than
orbital ones (see also Yoon et al. '16).

see, e.g., Molina & Bosch-Ramon '18,
Molina et al. '19, Bosch-Ramon &
Barkov '22 for orbital influence.

RMHD simulations of microquasar jets: stability

- Hydrodynamic-cold flow – particle dominated vs equipartition with magnetic field.
- Stellar wind from a massive O-type star ($dM/dt = 10^{-6} M_{\text{sun}} \text{ yr}^{-1}$).
- Numerical codes: Ratpenat (Perucho et al. 2010) RHD – Lóstrego (López-Miralles et al. 2022, 2023) RMHD.

	WIND	JET 1	JET 2	JET A	JET B	JET C
Jet Power (erg/s)		10^{35}	10^{37}	10^{35}	10^{37}	10^{37}
Magnetic power (erg/s)	0	0	0	$5 \cdot 10^{32}$	$5 \cdot 10^{34}$	$5 \cdot 10^{36}$
Velocity (cm/s)	$2 \cdot 10^8$	$1.7 \cdot 10^{10}$				
Density (g/cm ³)	$2.8 \cdot 10^{-15}$	$0.088 \rho_w$	$8.8 \rho_w$	$0.088 \rho_w$	$8.8 \rho_w$	$0.88 \rho_w$
ρ_m/ρ_g	0	0	0	1.03	1.03	1.56
$B_{j,m}^\phi$ (G)	-	0	0	$6.41 \cdot 10^1$	$6.41 \cdot 10^2$	$7.22 \cdot 10^3$

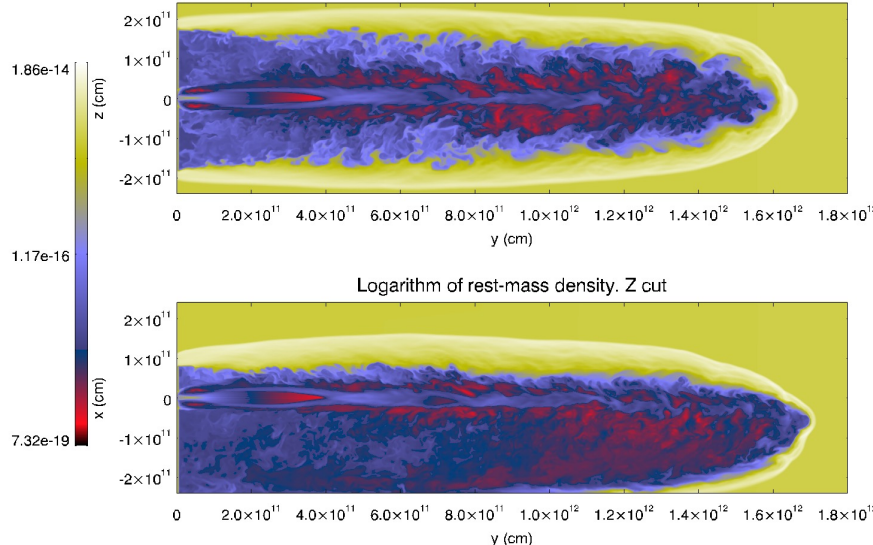
Perucho, Bosch-Ramon & Khangulyan 2010
 López Miralles et al. 2022

RMHD simulations of microquasar jets: stability

Jet 1 $t = 977$ s

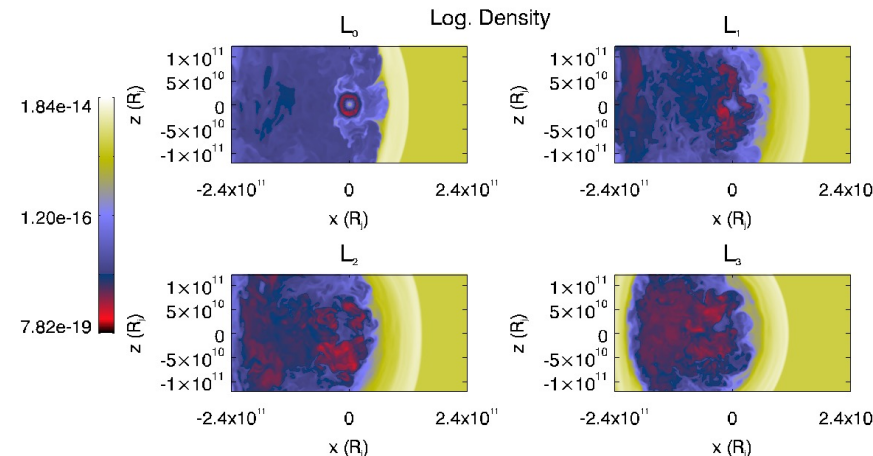
$d = 1.7 \cdot 10^{12}$ cm

Logarithm of rest-mass density. X cut



Perucho, Bosch-Ramon & Khangulyan 2010

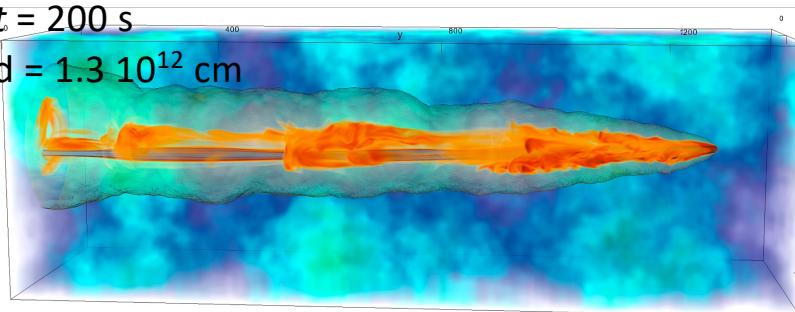
López Miralles et al. 2022



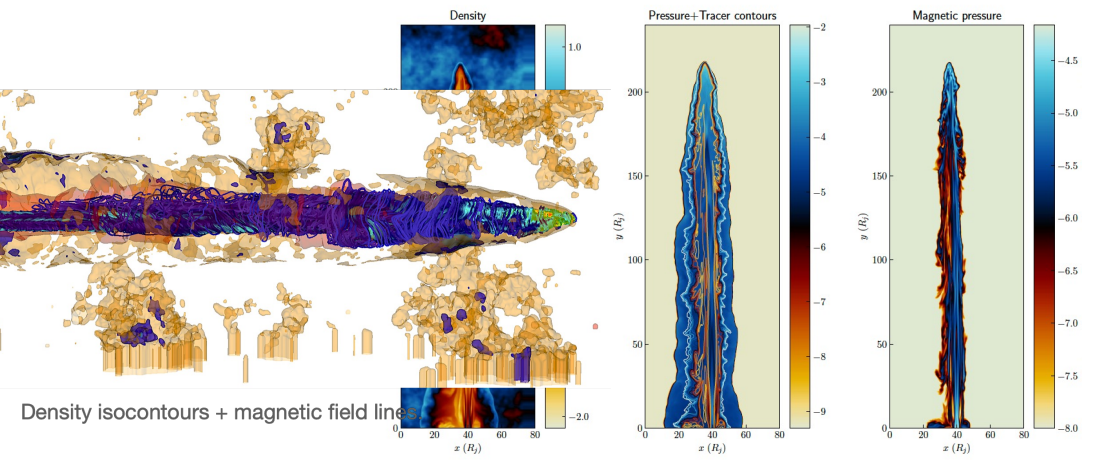
Jet A

$t = 200$ s

$d = 1.3 \cdot 10^{12}$ cm



3D render of jet A tracer and stellar wind clumps. A gas pressure contour (faint yellow) is included to show the position of the jet bow shock.

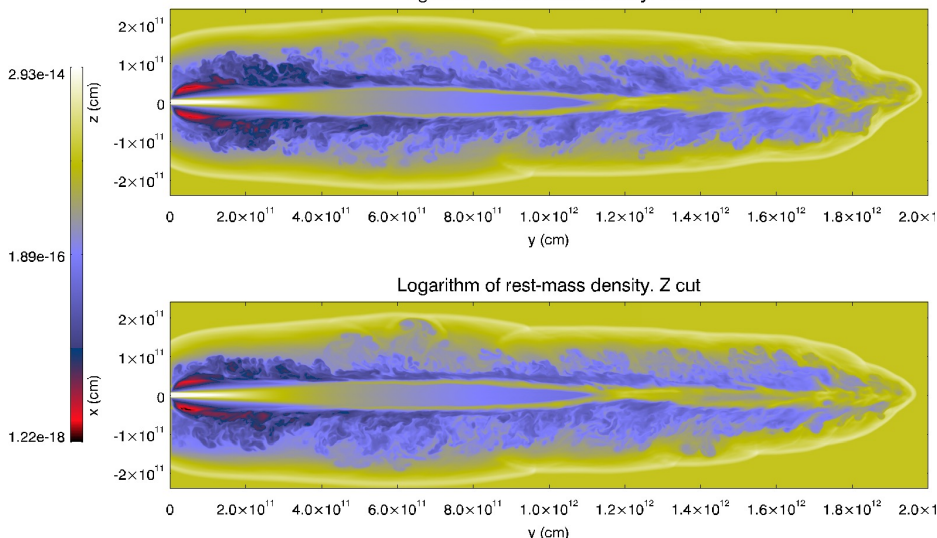


RMHD simulations of microquasar jets: stability

Jet 2 $t = 192$ s

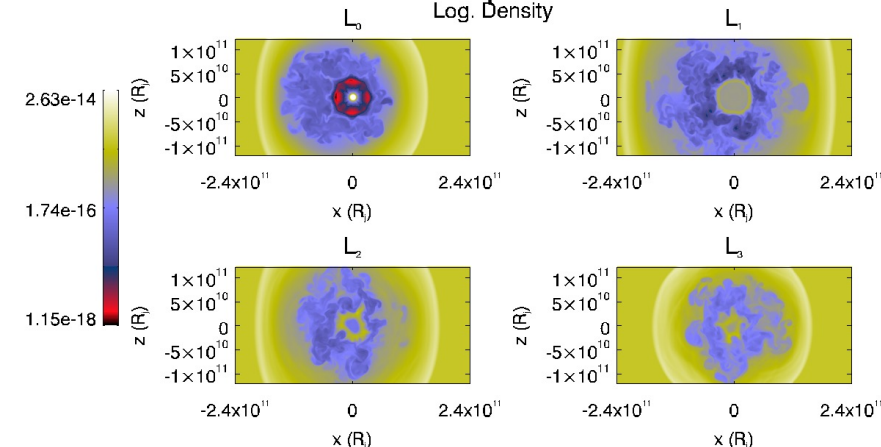
$$d = 2 \cdot 10^{12} \text{ cm}$$

Logarithm of rest-mass density. X cut



Perucho, Bosch-Ramon & Khangulyan 2010

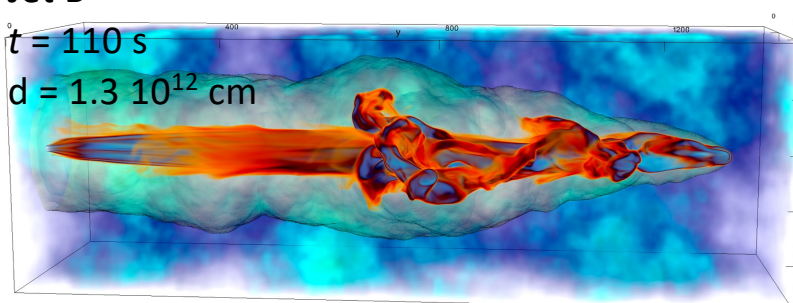
López Miralles et al. 2022



Jet B

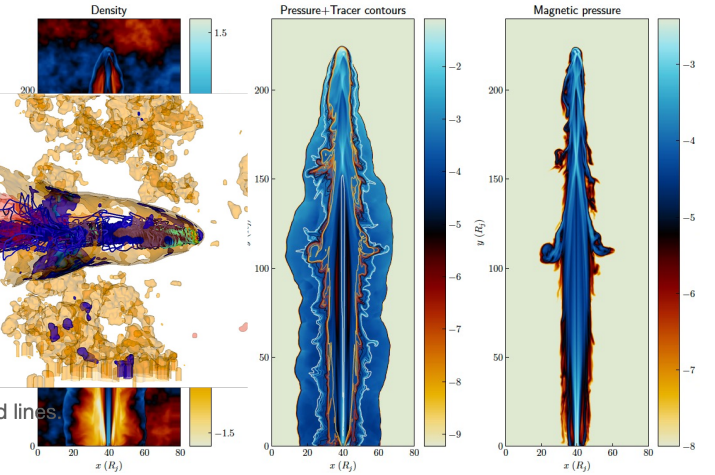
$t = 110$ s

$$d = 1.3 \cdot 10^{12} \text{ cm}$$



3D render of jet A tracer and stellar wind clumps. A gas pressure contour (faint yellow) is included to show the position of the jet bow shock.

Density isocontours + magnetic field lines.

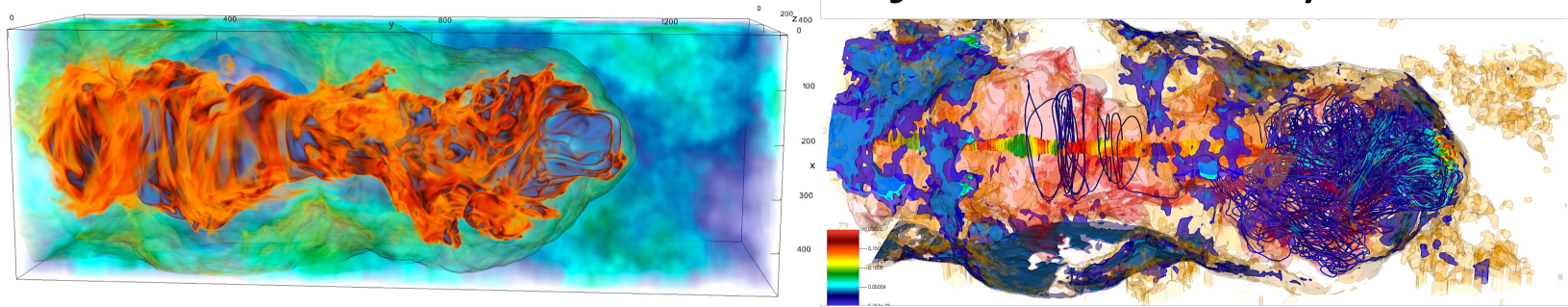


RMHD simulations of microquasar jets: stability

Jet C

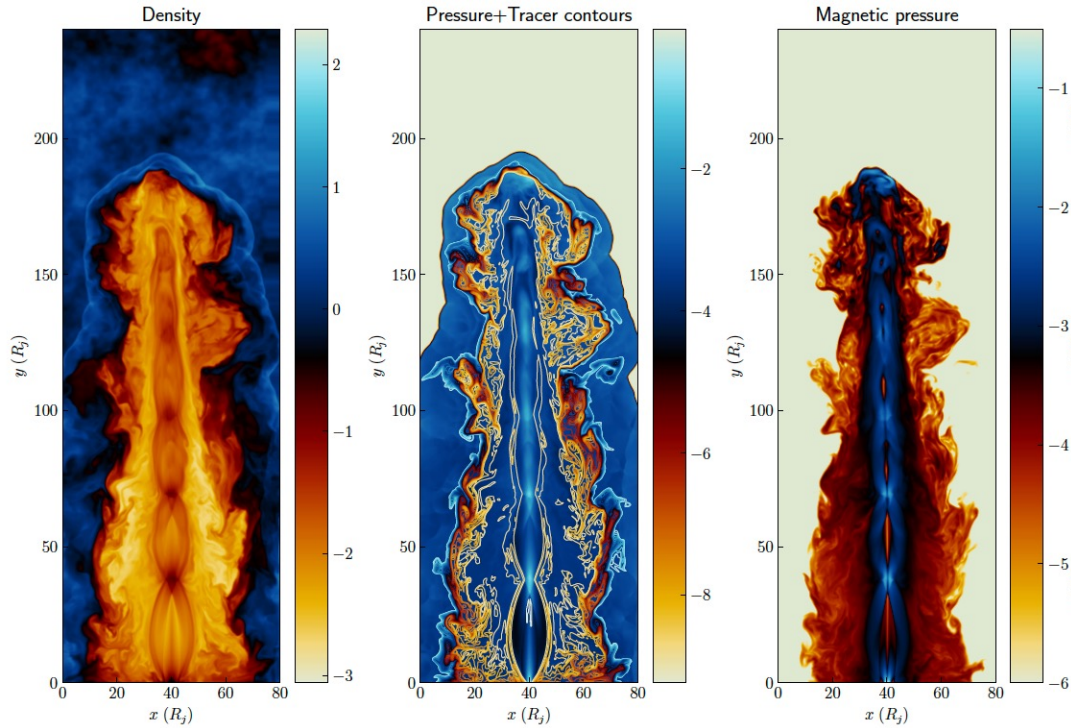
$t = 150$ s

$d = 1.2 \cdot 10^{12}$ cm

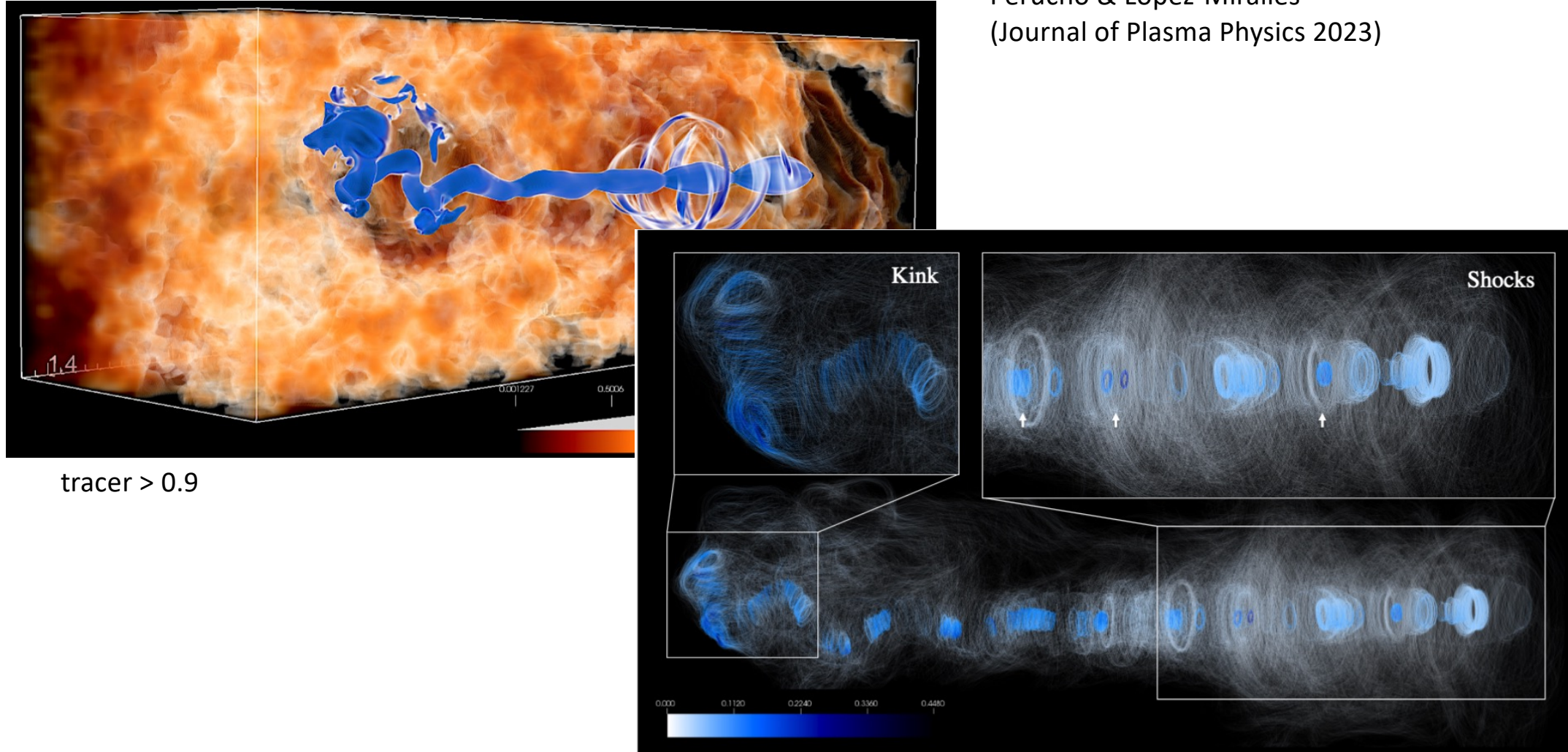


3D render of jet A tracer and stellar wind clumps. A gas pressure contour (faint yellow) is

Density isocontours + magnetic field lines.



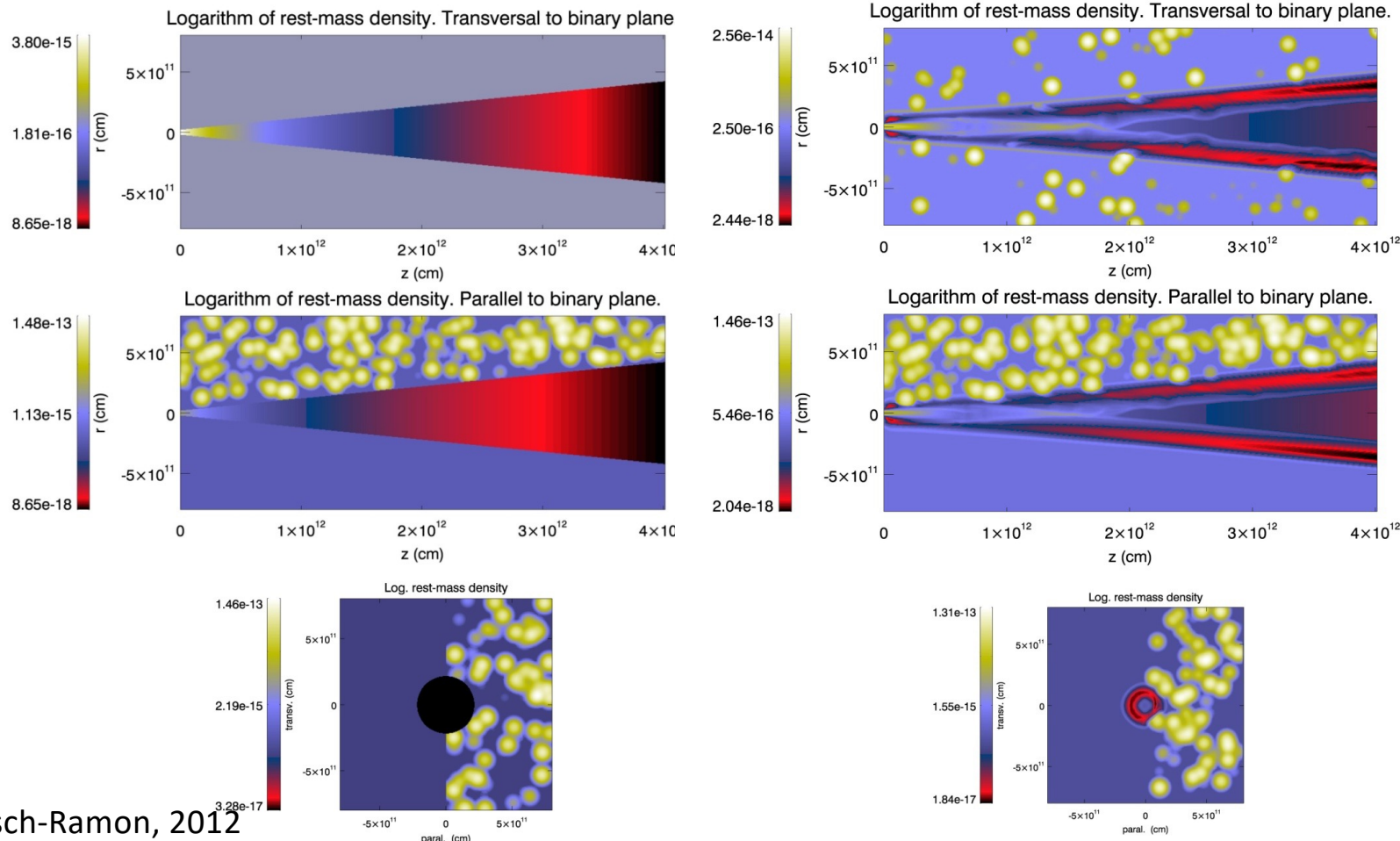
RMHD simulations of microquasar jets: stability



Simulations of jets in high-mass microquasars

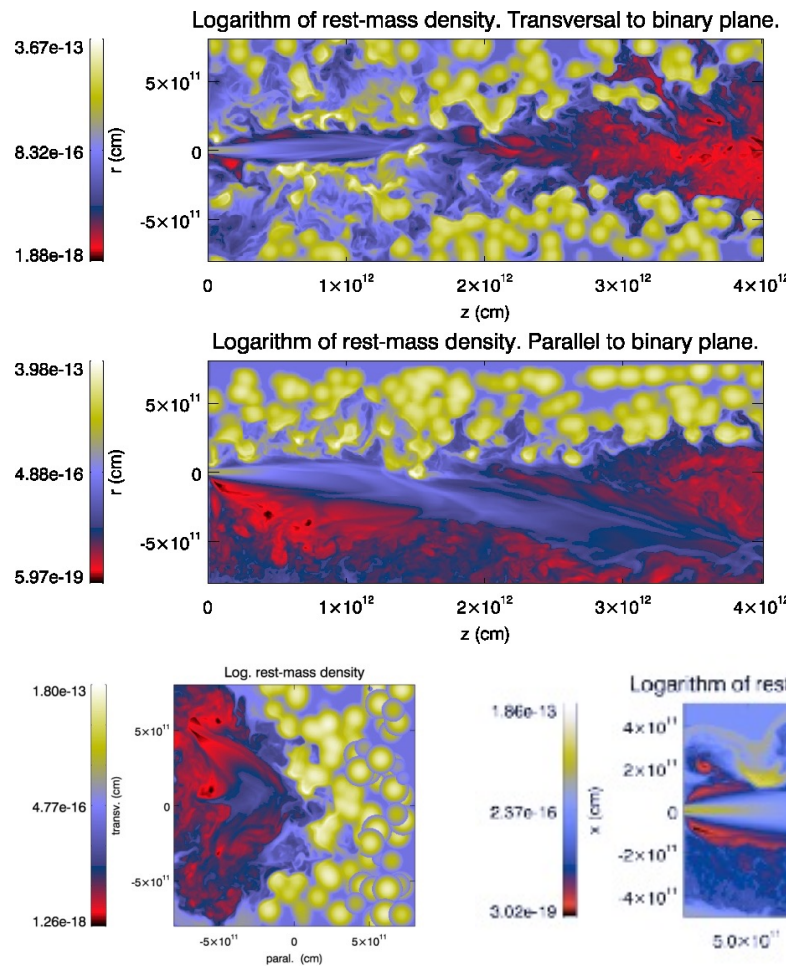
Wind-jet interaction in massive X-ray binaries: 3D simulations

Inhomogeneous wind

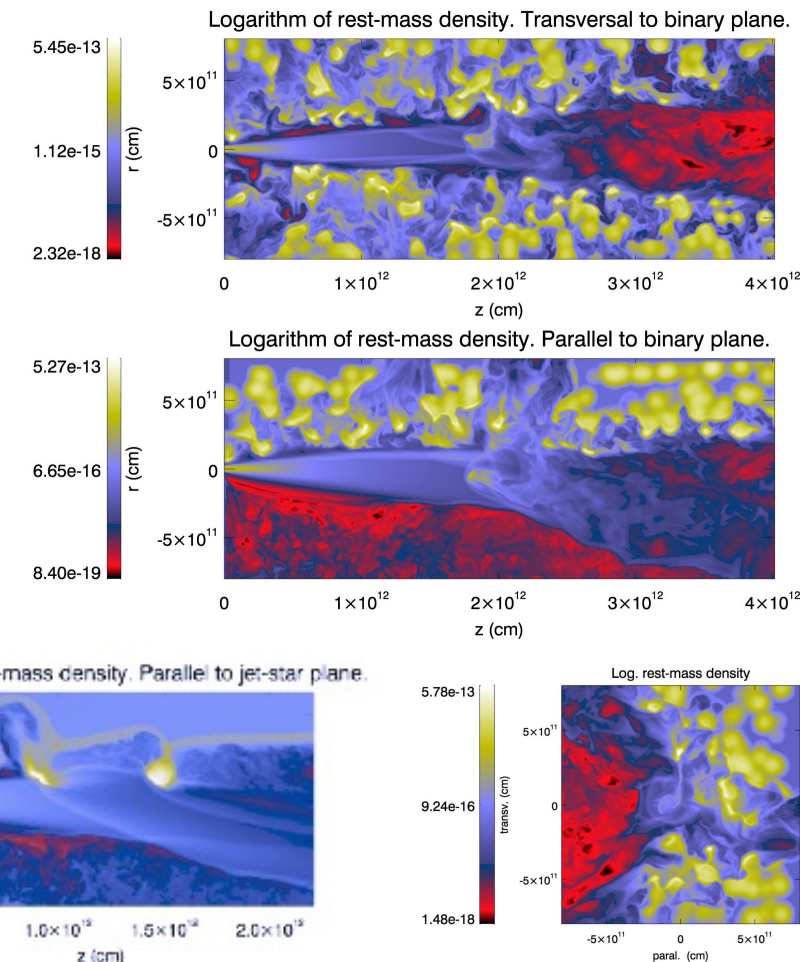


Simulations of jets in high-mass microquasars

Inhomogeneous wind. $P_j = 3 \times 10^{36} \text{ erg/s}$

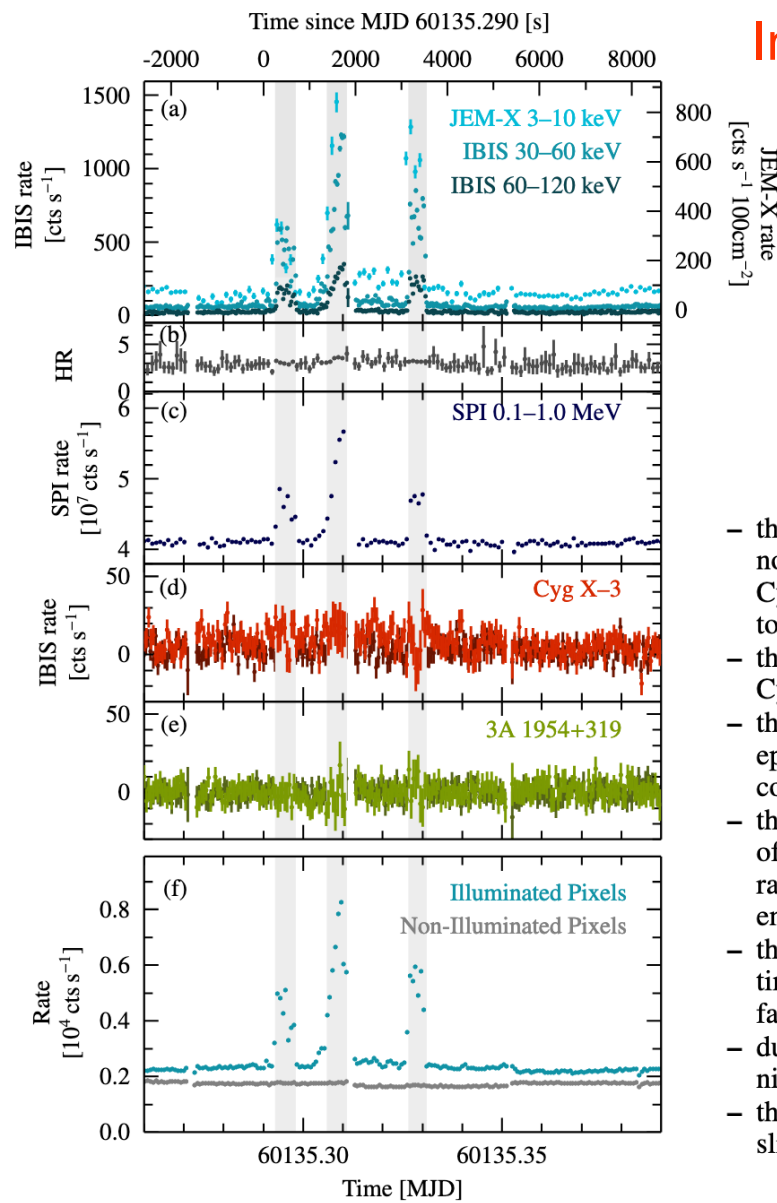


Inhomogeneous wind. $P_j = 10^{37} \text{ erg/s}$

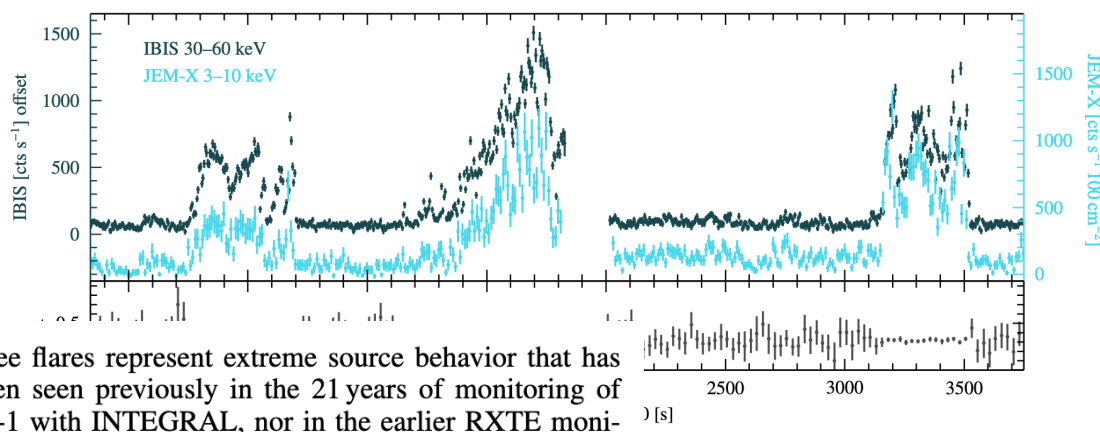


Perucho & Bosch-Ramon, 2012

Interpretation of an unprecedentedly bright X-ray flare in Cygnus X-1 observed by INTEGRAL



- the three flares represent extreme source behavior that has not been seen previously in the 21 years of monitoring of Cyg X-1 with INTEGRAL, nor in the earlier RXTE monitoring between 1997 and 2012,
- the flares occurred during the soft-intermediate state, when Cyg X-1 was moving towards the hard state,
- the flares occurred at orbital phase $\phi_{\text{orb}} = 0.01$ based on the ephemeris of Brocksopp et al. (1999), i.e., close to upper conjunction of the black hole,
- the flares have peak luminosities of 1–100 keV luminosity of $1.1\text{--}2.6 \times 10^{38}$ erg s⁻¹ ($4.1\text{--}9.7\% L_{\text{Edd}}$), a dynamic flux range of ~ 15 , and a duration of about 400 s each, with fluences of $3\text{--}5 \times 10^{40}$ erg each,
- the intensity profiles are complex with fast rise and decay times ~ 10 s for the first and third flare, and a slow rise and fast decay for the second flare,
- during all three flares the normalized rms variability is significantly increased,
- there is little spectral change in the hard X-rays, with only a slight softening > 30 keV (see ratio panel in Fig. 7).

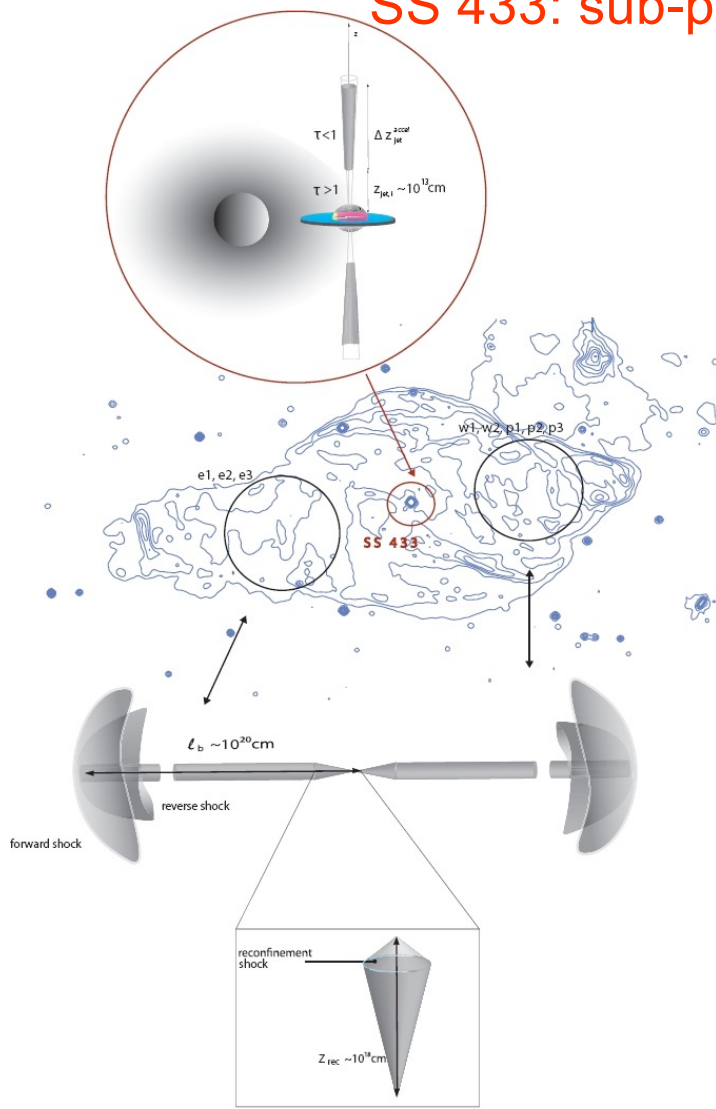


The time-scales of the flares (minutes) are incompatible with short term variability on the order of the Kepler timescales at the ISCO.

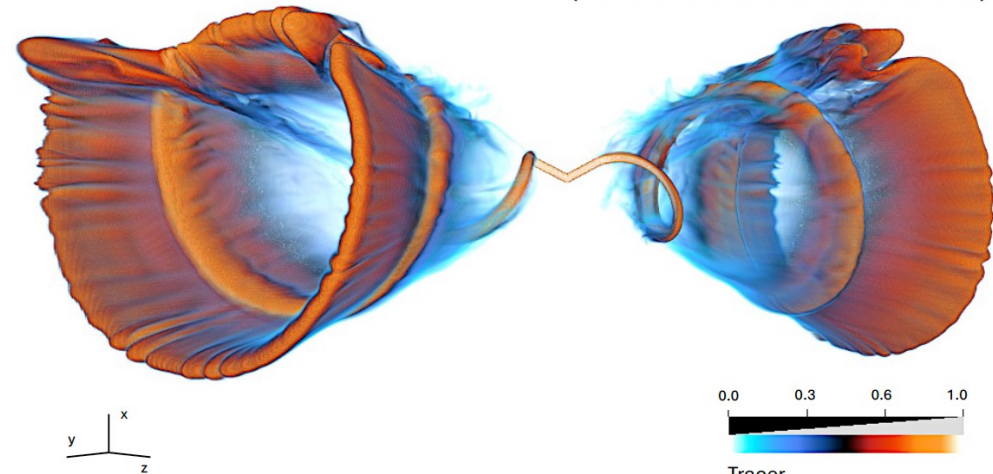
The interaction with stellar wind clumps is plausible (Araudo et al. 2009, Perucho & Bosch-Ramon 2012).

Thalhammer et al., submitted

SS 433: sub-parsec scales

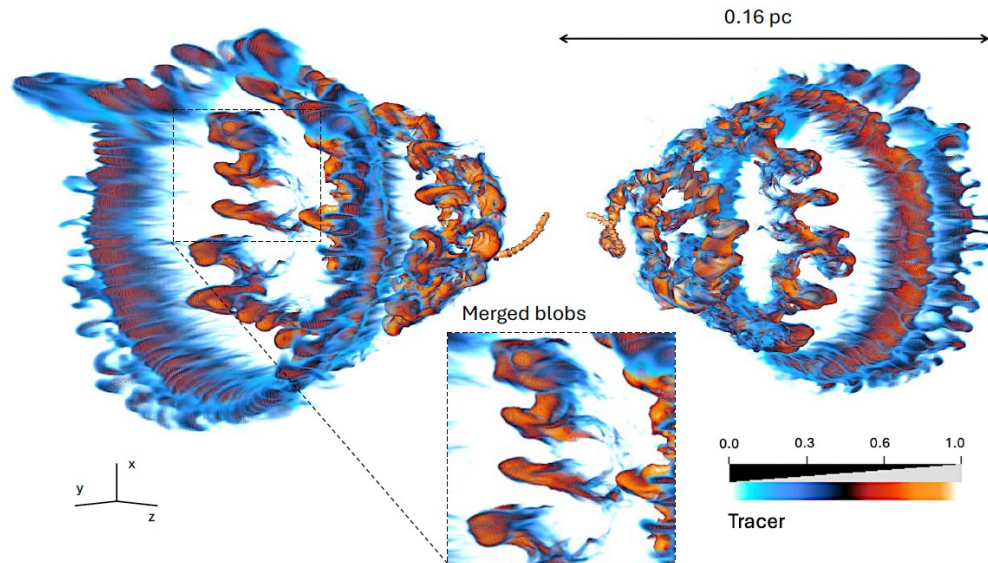


Continuous injection



López-Miralles et al. (in preparation)

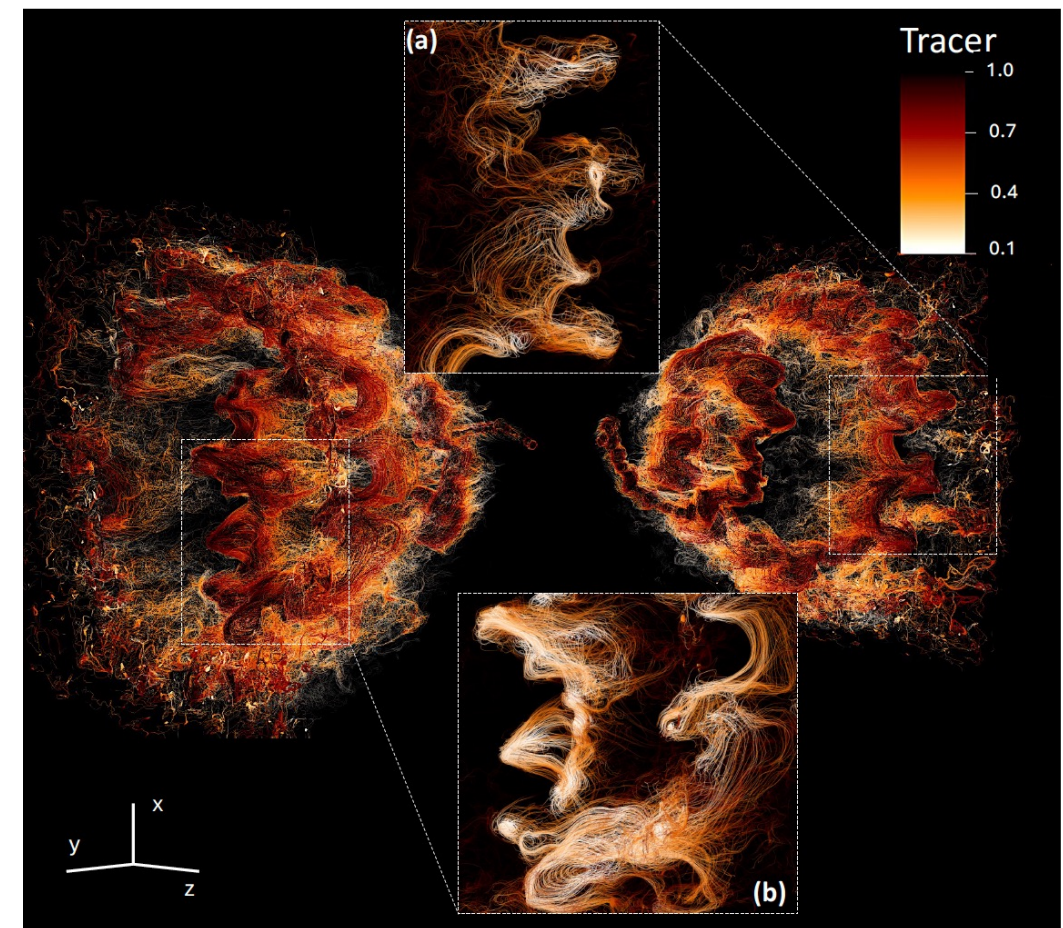
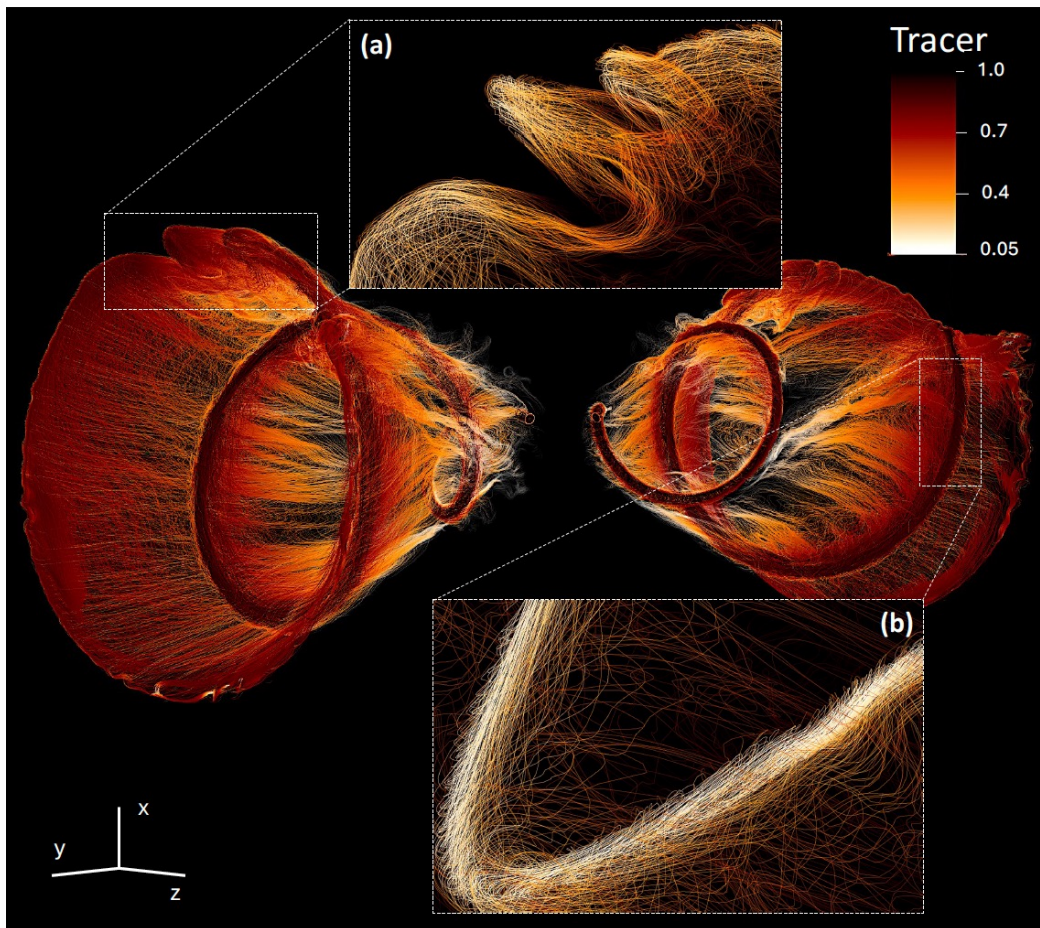
Blob-blob interactions



Bordas et al. 2010, Bordas 2020

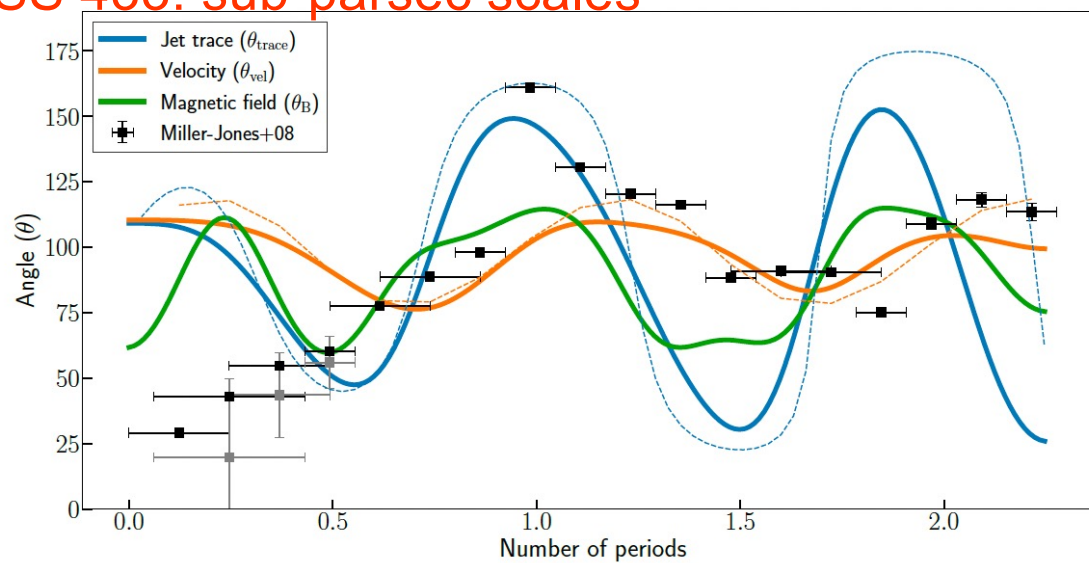
SS 433: sub-parsec scales

López-Miralles et al. (in preparation)

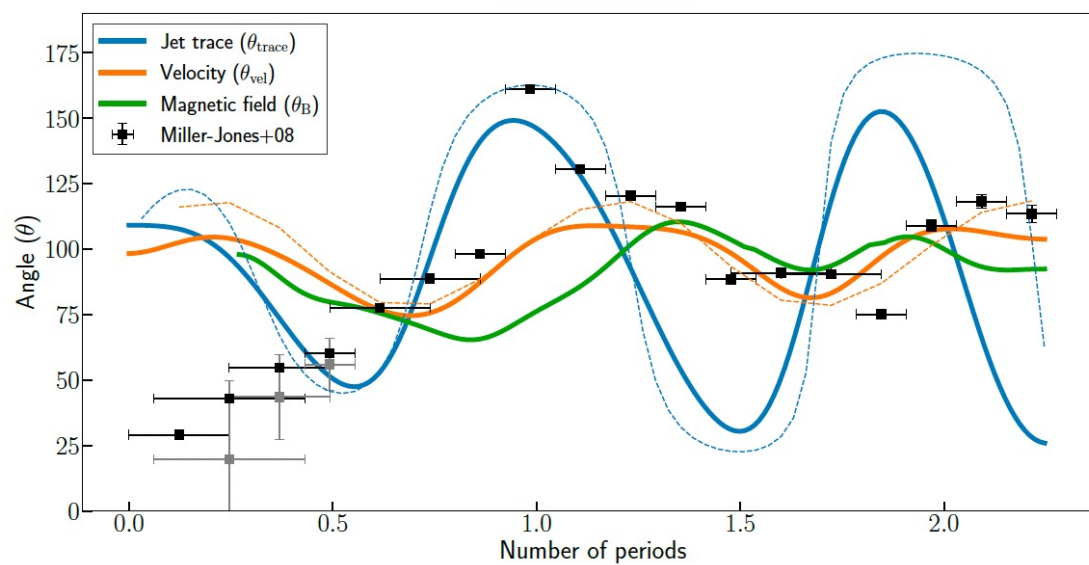


SS 433: sub-parsec scales

López-Miralles et al. (in preparation)



continuous flow



interacting blobs

CONCLUSIONS

- Bow shocks and reverse shocks at jet/ISM interaction can accelerate particles to VHE (e.g., Bordas et al. '09, Bosch-Ramon et al. '11).
 - Frustrated jets may not be observed in radio at large distances, but still be gamma-ray bright due to strong dissipation.
- Recollimation shocks within the cocoon, but also within the wind region. These shocks are generated in the binary region if (see Perucho & Bosch-Ramon 2008, Perucho et al. 2010, López-Miralles et al. 2022):
 - RHD: These strong shocks are candidate locations for particle acceleration and high-energy emission.
 - gamma-rays produced at such height above the orbital plane may be less absorbed by interaction with stellar photons.
 - RMHD: Recollimation shocks are not so strong! Still...
- Instabilities develop in RHD jets and RMHD with a relatively strong magnetic field: This can destroy the jet and generate turbulent regions.
- Only powerful jets ($P_j > 10^{37}$ erg/s) in massive binaries may be able to propagate collimated out of the binary region.
 - THIS NOW DEPENDS ON MAGNETIZATION!
- Inhomogenous winds could produce X-ray flares.
- SS 433 simulations show the relevant role of blob interactions to explain observed features at parsec scales.

Numerical simulations of relativistic jets

RHD equations

$$\frac{\partial D}{\partial t} + \nabla \cdot (D\mathbf{v}) = 0 \quad (\text{mass conservation})$$

$$\frac{\partial \mathbf{S}}{\partial t} + \nabla \cdot (\mathbf{S} \otimes \mathbf{v} + p\mathbf{I}) = 0 \quad (\text{momentum conservation})$$

$$\frac{\partial \tau}{\partial t} + \nabla \cdot (\mathbf{S} - D\mathbf{v}) = 0 \quad (\text{energy conservation})$$

STATE VECTOR

$$\mathbf{U} = (D, S^1, S^2, S^3, \tau)$$

DEFINITIONS

$D = \rho W$: relativistic rest-mass density.

$\mathbf{S} = \rho h W^2 \mathbf{v}$: relativistic momentum density.

$\tau = \rho h W^2 c^2 - p - \rho W c^2$: relativistic energy density.

\mathbf{v} : fluid flow velocity.

$W = 1/\sqrt{1 - \mathbf{v}^2/c^2}$: flow Lorentz factor.

RELATIVISTIC EFFECTS

$$h \geq 1 \quad (\epsilon \geq c^2)$$

$$W \geq 1 \quad (v \rightarrow c)$$

FLUX VECTORS

$$\mathbf{F}^i = (Dv^i, S^1 v^i + \delta^{1i}, S^2 v^i + \delta^{2i}, S^3 v^i + \delta^{3i}, S^i - Dv^i)$$

FLUID REST FRAME QUANTITIES

ρ : proper rest-mass density.

$h = 1 + \epsilon/c^2 + p/\rho c^2$: specific enthalpy.

ϵ : specific internal energy.

p : pressure.

RMHD equations

RMHD: Describes the dynamics of relativistic, electrically conducting fluids in the presence of magnetic fields.

Ideal RMHD: Absence of viscosity effects and heat conduction in the limit of infinite conductivity.

The relativistic description is easier in terms of the MAGNETIC FIELD FOUR-VECTOR IN THE LOCAL FLUID REST FRAME, $b^\mu = (b^0, \mathbf{b})$.

EQUATIONS

$$\frac{\partial D}{\partial t} + \nabla \cdot (D\mathbf{v}) = 0 \quad (\text{mass conservation})$$

$$\frac{\partial \mathbf{S}^*}{\partial t} + \nabla \cdot ((\mathbf{S}^* + b^0 \mathbf{b}) \otimes \mathbf{v} + p^* \mathbf{I} - \mathbf{b} \otimes \mathbf{b}) = 0$$

(momentum conservation)

$$\frac{\partial \tau^*}{\partial t} + \nabla \cdot (\mathbf{S}^* - D\mathbf{v}) = 0 \quad (\text{energy conservation})$$

$$\frac{\partial \mathbf{B}}{\partial t} - \nabla \times (\mathbf{v} \times \mathbf{B}) = 0 \quad (\text{induction equation})$$

$$\nabla \cdot \mathbf{B} = 0 \quad (\text{magnetic flux conservation})$$

DEFINITIONS

$$\mathbf{S}^* = \rho h^* W^2 \mathbf{v} - b^0 \mathbf{b}$$

$$\tau^* = \rho h^* W^2 c^2 - p^* - (b^0)^2 - \rho W c^2$$

$$\mathbf{B} = W(\mathbf{b} - b^0 \mathbf{v}/c)$$

FLUID REST FRAME QUANTITIES

$$p^* = p(1 + \beta); \beta: \text{magnetization, magnetic to internal (gas) energy density ratio.}$$

$$h^* = h + \sigma; \sigma: \text{magnetic to rest mass energy density ratio.}$$

RELATIVISTIC/MAGNETIC EFFECTS

$$\beta \geq 1$$

$$\beta, \sigma \geq 1: \text{force-free magnetic field; Poynting flux dominated flow}$$

$$b^0 = W(\mathbf{v} \cdot \mathbf{B}),$$

$$b^i = \frac{B^i}{W} + v^i b^0.$$

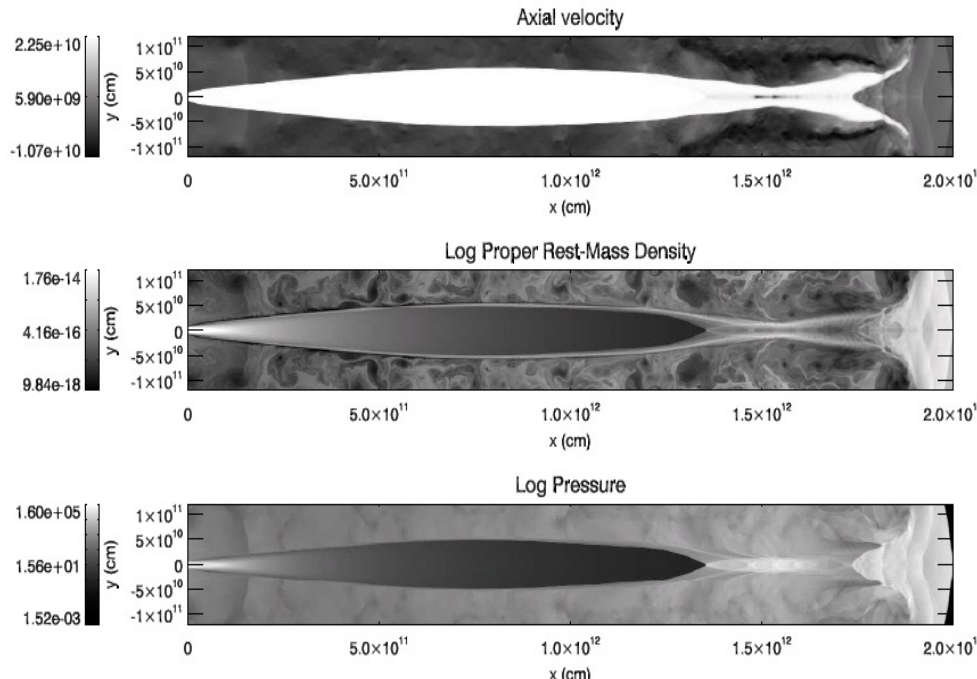
$$\sigma \equiv \frac{|b|^2}{\rho} \left(= \frac{2p_{\text{mag}}}{\rho} \right).$$

Simulations of jets in high-mass microquasars

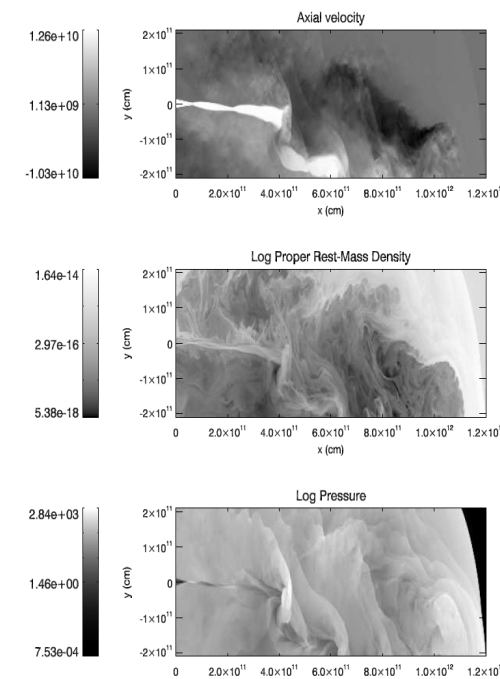
Wind-jet interaction in massive X-ray binaries: 2D simulations

2D simulations: Perucho & Bosch-Ramon 2008

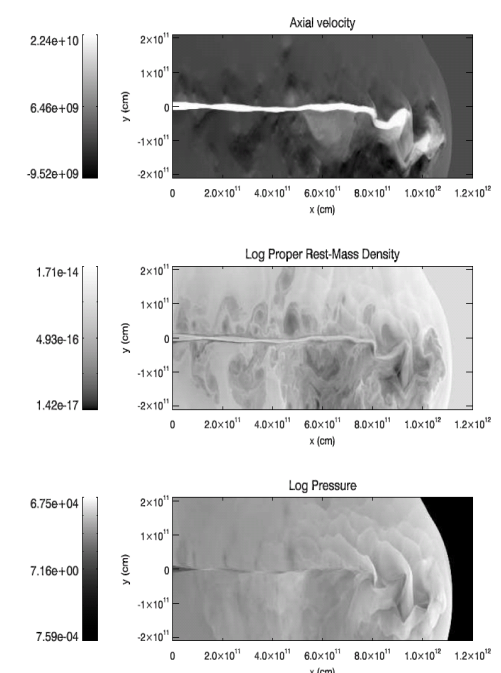
powerful jet (3×10^{37} erg/s)



weak jet (3×10^{34} erg/s)



intermediate jet (10^{36} erg/s)



320x2400 cells
20x300 R_j
+extended grid

1920x1600 cells
120x200 R_j
+extended grid

